

# Proposing a New Velocity Profile for Continuous X-Ray Tube Motion in Digital Breast Tomosynthesis

Raymond J. Acciavatti, Predrag R. Bakic, and Andrew D. A. Maidment  
University of Pennsylvania, Department of Radiology, 3400 Spruce St., Philadelphia PA 19104  
E-mail: raccia@seas.upenn.edu, {Predrag.Bakic | Andrew.Maidment}@uphs.upenn.edu

## ABSTRACT

In digital breast tomosynthesis (DBT), a 3D image of the breast is generated from x-ray projections at various angles. There are two mechanisms for acquiring projection images in DBT, step-and-shoot motion and continuous tube motion. The benefit of continuous tube motion is shorter scan time and hence less patient motion; the trade-off is focal spot blurring. To minimize focal spot blurring in a system with continuous tube motion, this study proposes a new velocity profile for the x-ray tube during the scan. Unlike existing systems for which the x-ray tube has constant angular velocity, we investigate a smoothly-varying tube velocity that approaches zero during each projection and is larger between projections. With this unique design, the filtered backprojection reconstruction of a sinusoidal test object was calculated, and modulation was determined at various frequencies. It is shown that the newly proposed tube velocity yields increased modulation in the reconstruction relative to a conventional system with continuous tube motion. The modulation in the re-designed system differs minimally from an analogous step-and-shoot system operated with the same scan time. This improvement in image quality was validated with reconstructions of microcalcifications in computer breast phantoms. It is known that continuous tube motion reduces the contrast of microcalcifications relative to step-and-shoot systems; we show that the newly proposed tube motion increases the contrast of microcalcifications compared to conventional continuous tube motion. In conclusion, this work proposes a strategy for optimizing the velocity of tube motion in DBT.

**Keywords:** Digital breast tomosynthesis (DBT), continuous tube motion, step-and-shoot motion, patient motion, image reconstruction, filtered backprojection, modulation, optimization.

## 1. INTRODUCTION

In digital breast tomosynthesis (DBT), one benefit of continuous tube motion (CTM) over step-and-shoot motion (SSM) is shorter scan time. Although the short scan time reduces the potential for patient motion in CTM systems, it comes with the trade-off of increased focal spot (FS) blurring during the exposure time of each projection. Previous studies have shown that the impact of FS blurring can be seen in the modulation transfer function (MTF). In simulating the Siemens DBT system, Shaheen *et al.* found that FS blurring decreases MTF by 10% at 2 line pairs per millimeter (lp/mm) and 50% at 6 lp/mm.<sup>1</sup>

Because the MTF degradation due to FS blurring is most pronounced at high frequencies, the greatest loss of image quality is expected in reconstructions of small objects, such as microcalcifications. In simulating microcalcifications as small spheres with 250  $\mu\text{m}$  diameter, Shaheen *et al.* found nearly 10% loss in peak contrast due to FS blurring.<sup>1</sup> Our own previous work also demonstrated loss of modulation in the reconstruction due to FS blurring, and showed that the frequency at which the modulation is first zero increases with scan time.<sup>2</sup>

In existing CTM systems, manufacturers configure the x-ray tube with constant angular velocity. To minimize FS blurring, we propose a new velocity profile for the x-ray tube. We model a tube velocity that is large between projections but approaches zero during each projection to minimize FS blurring. Importantly, this velocity profile is smooth, so that there is no abrupt start-and-stop motion that would make a fast acquisition time prohibitive. This technical innovation should allow a CTM system to have a short scan time and hence less patient motion than a SSM system, while no longer suffering from the trade-off of FS blurring during each projection.

Our previous studies introduced a conceptual test object known as a sine plate for evaluating image quality in DBT.<sup>2-6</sup> This object is a thin strip whose attenuation coefficient varies sinusoidally. To assess image quality in DBT, the reconstruction of a sine plate can be calculated at various input frequencies. Modulation is found by comparing the amplitude of the reconstruction against the attenuation coefficient of the object. This work studies whether the newly proposed x-ray tube velocity increases modulation in a CTM system. It has been suggested that tube motion reduces the contrast of microcalcifications relative to SSM systems. Using computer breast phantoms, we also investigate whether re-designing the tube velocity increases the contrast of microcalcifications compared with conventional CTM.

## 2. METHODS

To optimize a system with continuous tube motion, we propose that the angular velocity of the x-ray tube varies sinusoidally with time, as shown in Figure 1. The tube velocity is large between projections, and smoothly falls to a low value ( $\omega_{\min}$ ) during the exposure time of each projection to minimize FS blurring. Assuming that the tube rotates within the plane of the chest wall, the differential equation relating the tube angle  $\psi$  to time  $T$  is

$$\frac{d\psi}{dT} = \frac{1}{2} [\omega_{\max} + \omega_{\min} - (\omega_{\max} - \omega_{\min}) \cos(2\pi\Omega T)], \quad (1)$$

where  $\Omega$  is the temporal frequency of the angular velocity of the x-ray tube, and  $\omega_{\min}$  and  $\omega_{\max}$  denote the minimum and maximum angular velocities of the x-ray tube, respectively. To minimize FS blurring, the troughs of this waveform should occur at the central time points,  $T_n$ , during the exposure time  $\tau$  of all of the  $n$  projections. According to Eq. (1), this condition is satisfied provided that  $\cos(2\pi\Omega T_n) = 1$ , or  $\Omega T_n = n$ , where  $T_n$  is calculated in our previous work<sup>2</sup> as

$$T_n = n(\tau + \Delta T), \quad \Delta T = \frac{T_t - N\tau}{N-1}, \quad -\frac{N-1}{2} \leq n \leq \frac{N-1}{2}, \quad n \in \mathbb{Z}. \quad (2)$$

In these expressions,  $T_t$  is the total scan time,  $\Delta T$  models the time difference between any two consecutive projections, and  $N$  denotes the total number of projections. From Eq. (2), it follows that  $\Omega = (N-1)/(T_t - \tau)$ . Under this constraint for  $\Omega$ , one can solve the differential equation in Eq. (1)

$$\psi(T) = A + \frac{T}{2} (\omega_{\max} [1 - \text{sinc}(2\Omega T)] + \omega_{\min} [1 + \text{sinc}(2\Omega T)]), \quad \text{sinc}(u) \equiv \frac{\sin(\pi u)}{\pi u}, \quad (3)$$

where  $A$  is the constant of integration. Following the convention established in our previous work,<sup>2</sup> the time  $T$  ranges between  $-T_t/2$  and  $T_t/2$ , so that the central projection ( $\psi = 0$ ) occurs at the time  $T = 0$ . Based on this convention, it is clear that  $A = 0$ . To determine  $\omega_{\min}$  and  $\omega_{\max}$ , one must introduce boundary conditions for the angular sweep of the x-ray tube per projection ( $\Psi$ ). From the definition of  $\Psi$ , it follows that

$$\psi\left(\frac{\tau}{2}\right) - \psi\left(-\frac{\tau}{2}\right) = \Psi, \quad (4)$$

and hence

$$\omega_{\max} = \frac{2\Psi - \tau\omega_{\min} [1 + \text{sinc}(\Omega\tau)]}{\tau [1 - \text{sinc}(\Omega\tau)]}. \quad (5)$$

An additional boundary condition is the total angular sweep of the x-ray tube during the scan time  $T_t$

$$\psi\left(\frac{T_t}{2}\right) - \psi\left(-\frac{T_t}{2}\right) = \left[\left(\frac{N-1}{2}\right)\Delta\psi + \frac{\Psi}{2}\right] - \left[-\left(\frac{N-1}{2}\right)\Delta\psi - \frac{\Psi}{2}\right] = (N-1)\Delta\psi + \Psi, \quad (6)$$

giving

$$\omega_{\max} = \frac{2[\Psi + (N-1)\Delta\psi] - T_i \omega_{\min} [1 + \text{sinc}(\Omega T_i)]}{T_i [1 - \text{sinc}(\Omega T_i)]}, \quad (7)$$

where  $\Delta\psi$  is the step angle (*i.e.*, the angular spacing between projections). Combining Eqs. (5) and (7) yields

$$\Psi = \frac{[1 - \text{sinc}(\Omega\tau)](N-1)\Delta\psi + \omega_{\min} T_i [\text{sinc}(\Omega\tau) - \text{sinc}(\Omega T_i)]}{\frac{T_i}{\tau} [1 - \text{sinc}(\Omega T_i)] - [1 - \text{sinc}(\Omega\tau)]} \quad (8)$$

and

$$\omega_{\max} = \frac{2(N-1)\Delta\psi - \omega_{\min} (T_i [1 + \text{sinc}(\Omega T_i)] - \tau [1 + \text{sinc}(\Omega\tau)])}{T_i [1 - \text{sinc}(\Omega T_i)] - \tau [1 - \text{sinc}(\Omega\tau)]}. \quad (9)$$

By decoupling the relationship between  $\omega_{\max}$  and  $\Psi$ , Eq. (9) allows us to determine the focal spot position at all time points during the scan based on Eq. (3).

In earlier studies, we investigated a test object known as a sine plate as a framework for assessing image quality in DBT. This object, which is diagrammed in Figure 2 of our previous paper,<sup>2</sup> is a thin strip whose attenuation coefficient varies sinusoidally. Increasing the frequency of the sine plate simulates small closely-spaced structures such as microcalcifications. Using Eq. (3), we can calculate the reconstruction of a sine plate for our proposed tube motion following the formulae derived in our previous work.

### 3. RESULTS

#### 3.1 Model of Modulation for Various Forms of X-Ray Tube Motion

Figure 1(a) illustrates how the x-ray tube velocity in the newly proposed design (CTM\*) varies with time in a DBT system with continuous tube motion, assuming that  $N = 15$ ,  $\Delta\psi = 1.07^\circ$ ,  $\tau = 50.0$  ms,  $T_i = 3.5$  s, and  $\omega_{\min} = 0$ . The plot shows three of the 15 time points during which x-ray projections are acquired, corresponding to the troughs at which the tube velocity vanishes. In Figure 1(c), the dependency of the tube angle  $\psi$  on time  $T$  is investigated for this tube velocity profile. This plot shows that the tube angle  $\psi$  increases with time, but is approximately constant over three plateaus corresponding to the time points during which x-ray projections are acquired. Since the x-ray tube motion is negligible along these plateaus, FS blurring is minimal.

In Figures 1(b) and 1(d), the effect of increasing the minimum x-ray tube angular velocity ( $\omega_{\min}$ ) is investigated by letting  $\omega_{\min} = 2.17^\circ/\text{s}$ . This value corresponds to one-half of the x-ray tube velocity ( $\omega_{\text{CTM}}$ ) for a conventional CTM system operated with the same acquisition parameters. Our previous work showed that  $\omega_{\text{CTM}}$  is given by the expression<sup>2</sup>

$$\omega_{\text{CTM}} = \left( \frac{N-1}{T_i - \tau} \right) \Delta\psi. \quad (10)$$

In this example,  $\omega_{\text{CTM}}$  is  $4.34^\circ/\text{s}$ . Since the tube velocity does not fall exactly to zero [Figure 1(b)], the tube motion during each projection is more pronounced in Figure 1(d) than in Figure 1(c). This result indicates that the minimum tube velocity should be as close to zero as possible to minimize FS blurring. Figure 1 shows that there is a trade-off between  $\omega_{\min}$  and  $\omega_{\max}$  as  $\omega_{\min}$  is reduced. In particular, a decrease in the value of  $\omega_{\min}$  requires an increase in the value of  $\omega_{\max}$ . In Figure 1(b) for which  $\omega_{\min} = 2.17^\circ/\text{s}$ ,  $\omega_{\max}$  is  $6.51^\circ/\text{s}$ . By contrast, in Figure 1(a) for which  $\omega_{\min} = 0$ ,  $\omega_{\max}$  is  $8.68^\circ/\text{s}$ .

In an experimental system, mechanical considerations may place a limit on the maximum x-ray tube velocity that is achievable. To illustrate that this mechanical constraint also has an effect on  $\omega_{\min}$ , Figure 2(a) explicitly shows the coupling between  $\omega_{\max}$  and  $\omega_{\min}$ . In the figure,  $\omega_{\max}$  and  $\omega_{\min}$  are normalized by the tube velocity for conventional CTM ( $\omega_{\text{CTM}}$ ). In order to achieve the smallest possible FS blurring ( $\omega_{\min} = 0$ ), the maximum x-ray tube velocity must be twice

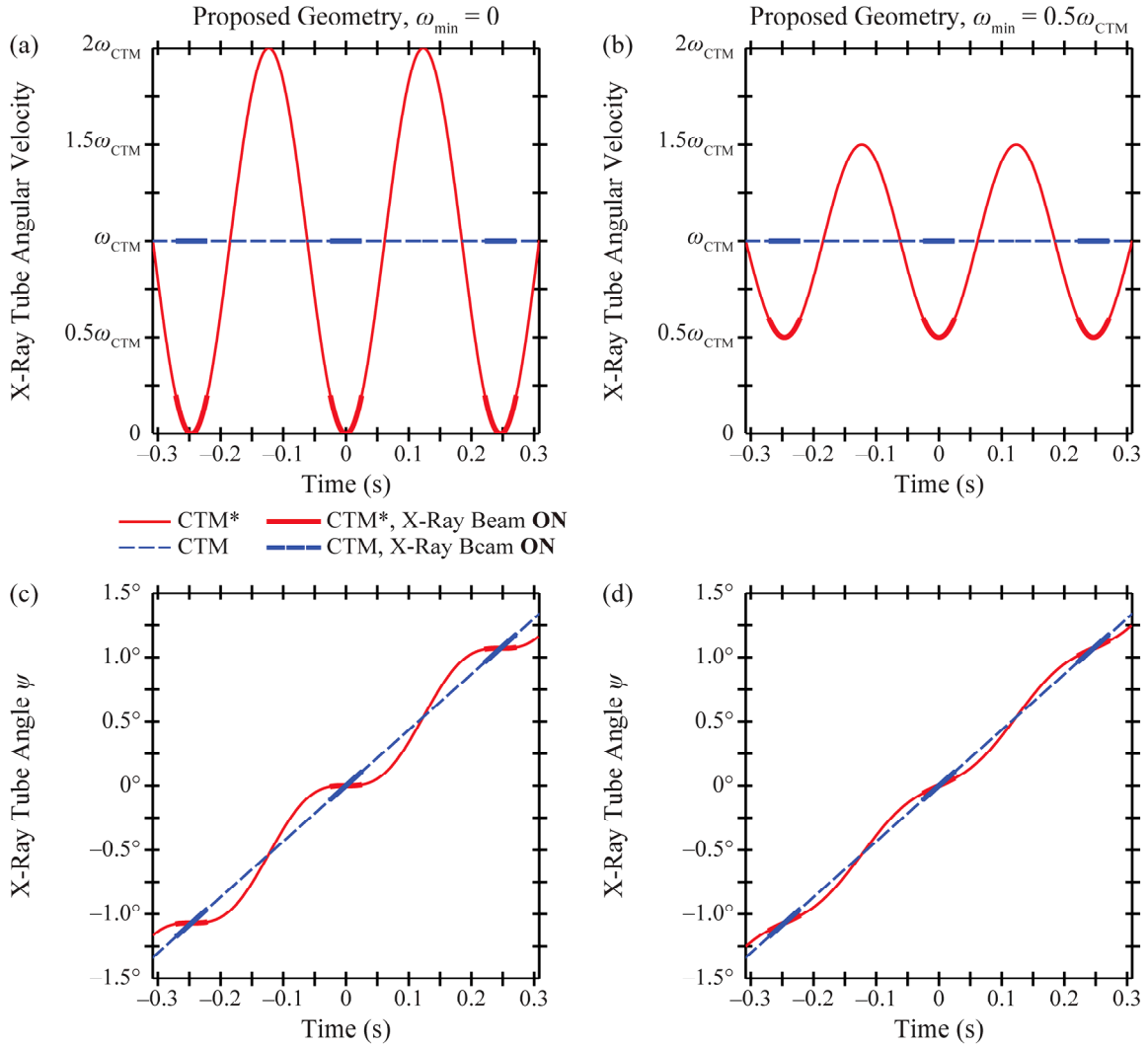


**Figure 1.** (a)-(b) Assuming that  $N = 15$ ,  $\Delta\psi = 1.07^\circ$ ,  $\tau = 50.0$  ms, and  $T_t = 3.5$  s, the angular velocity of the x-ray tube is plotted versus time. In the newly proposed system (CTM\*), the tube velocity approaches zero during each projection to minimize FS blurring. The parameter  $\omega_{\min}$  controls the minimum tube velocity, which can be expressed as a multiple of the tube velocity for conventional CTM ( $\omega_{\text{CTM}}$ ). (c)-(d) In the CTM\* geometry, the tube angle  $\psi$  is approximately constant over plateaus corresponding to time points during the projections. FS blurring is more pronounced with increasing  $\omega_{\min}$ .

the value for conventional CTM (*i.e.*,  $\omega_{\max} = 2\omega_{\text{CTM}}$ ). Achieving this maximum tube velocity is thus the mechanical constraint for optimizing image quality with the newly proposed design.

To further illustrate the effect of  $\omega_{\min}$  on FS blurring, Figure 2(b) shows the tube sweep  $\Psi$  per projection [Eq. (8)] as a function of  $\omega_{\min}$ . A schematic diagram of  $\Psi$  is given in Figure 3. In order to compare the tube sweep per projection in the newly proposed geometry against conventional CTM,  $\Psi$  is normalized by the corresponding value for conventional CTM. Our previous work showed that  $\Psi_{\text{CTM}}$  can be calculated as

$$\Psi_{\text{CTM}} = \left( \frac{N-1}{T_t - \tau} \right) \tau \Delta\psi. \quad (11)$$

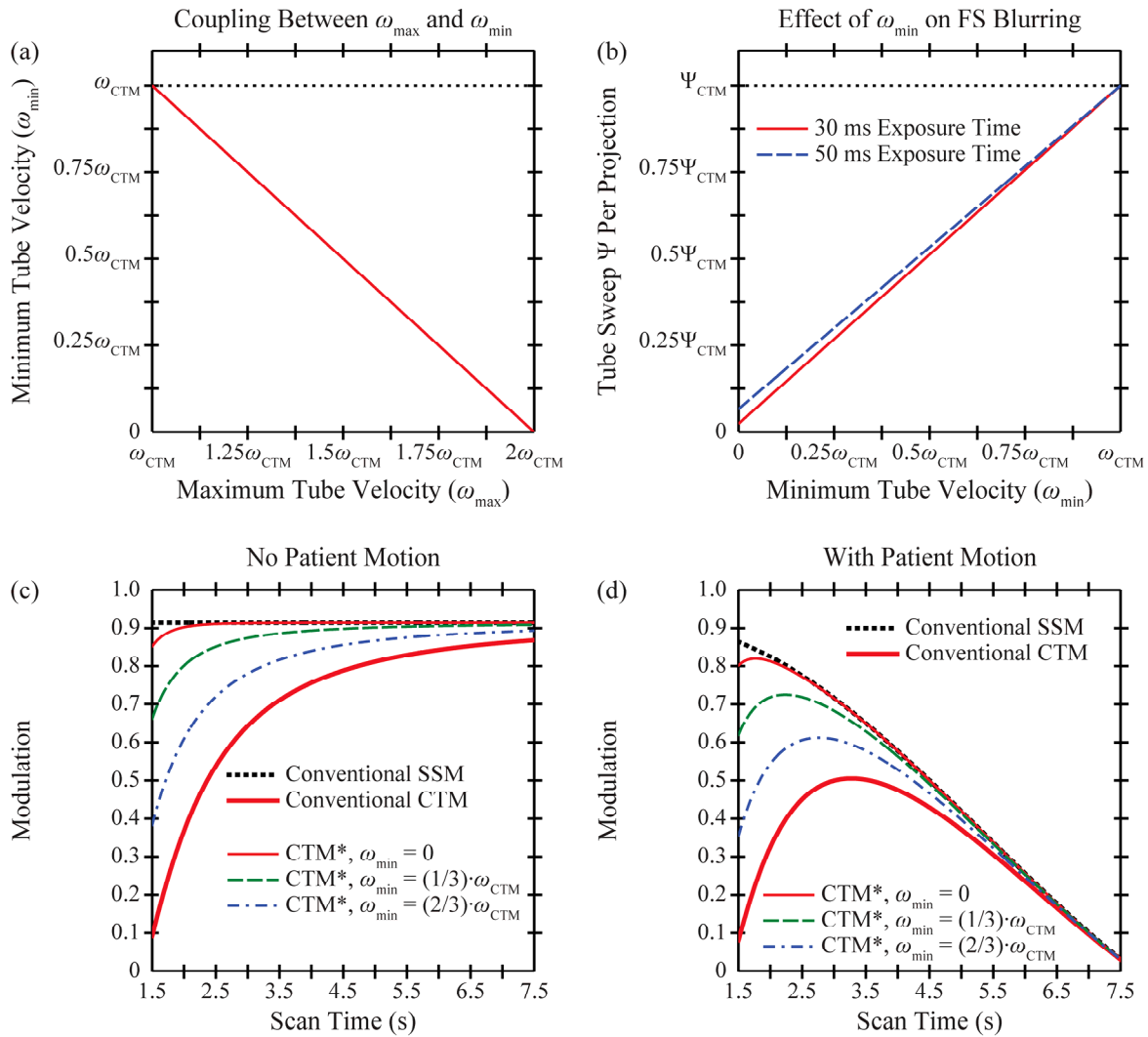


**Figure 2.** (a) In the newly proposed design, the maximum and minimum tube velocities are coupled ( $\omega_{\max}$  and  $\omega_{\min}$ , respectively). If mechanical considerations place a constraint on the maximum tube velocity that is achievable, the minimum tube velocity is also constrained according to this plot. (b) The tube sweep  $\Psi$  per projection provides a measure of FS blurring in a system with continuous tube motion. This plot demonstrates that FS blurring is more pronounced with increasing  $\omega_{\min}$ , as expected from Figure 1. (c) In a system with no patient motion, the newly proposed design (CTM\*) yields increased modulation relative to conventional CTM. The improvement in modulation is most pronounced at values of  $\omega_{\min}$  that approach zero. (d) With tube motion and patient motion occurring simultaneously, modulation is maximized by an intermediate scan time.

Figure 2(b) demonstrates that FS blurring increases as  $\omega_{\min}$  is increased. This result is expected, since the x-ray tube motion during each projection is more pronounced with increasing  $\omega_{\min}$  (Figure 1). Although Figure 1 assumes an exposure time of 50.0 ms, Figure 2(b) investigates an additional exposure time (30.0 ms). The two exposure times correspond to the mean and maximum values for the Selenia Dimensions DBT system (Hologic Inc., Bedford, MA), which is currently the only DBT system with FDA approval (as of February 2013). For the two respective exposure times of 30.0 and 50.0 ms, Figure 2(b) illustrates that the tube sweep per projection attains 2.4% and 6.6% of the corresponding value for conventional CTM provided that  $\omega_{\min} = 0$ . By contrast, the tube sweep  $\Psi$  attains 51.2% and 53.3% of the corresponding value for conventional CTM provided that  $\omega_{\min} = 0.5\omega_{\text{CTM}}$ . The smaller tube sweep per projection in the newly proposed design yields less FS blurring than conventional CTM. An additional property made clear in Figure 2(b) is that, for all values of  $\omega_{\min}$ , FS blurring is minimized as the exposure time is reduced.

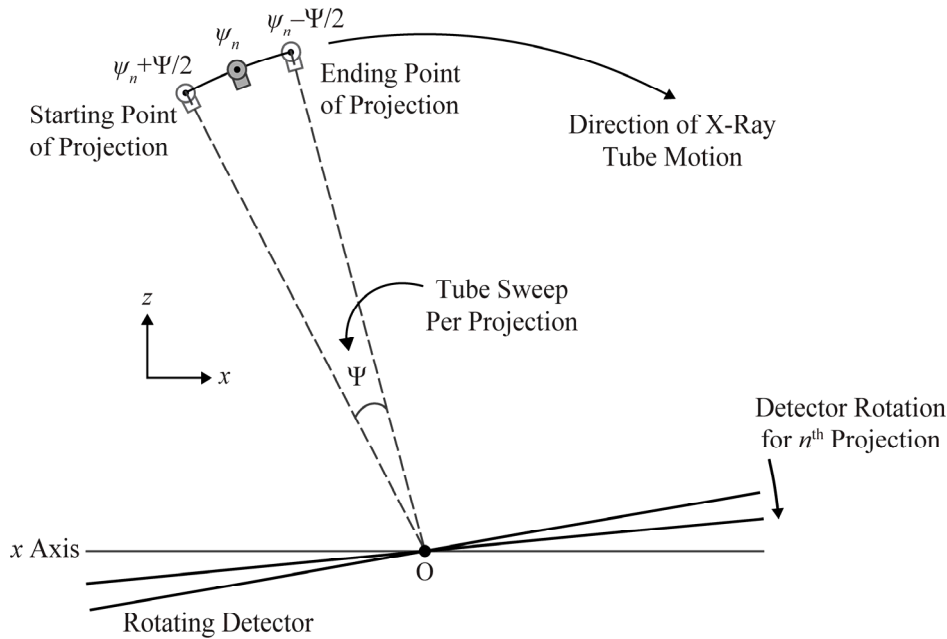


**Figure 3.** The tube sweep per projection ( $\Psi$ ) provides a measure of FS blurring in a system with continuous tube motion. The relationship between  $\Psi$  and  $\omega_{\min}$  is studied in Figure 2(b).

To assess the improvements in image quality with the newly proposed design, we determine the modulation in the reconstruction of a sine plate. Modulation is calculated as the ratio of signal in the reconstruction to the attenuation coefficient of the object. For high image quality, modulation should be preserved. In Figure 2(c), modulation is plotted versus total scan time ( $T$ ) for a 0.5 mm thick sine plate placed 50.0 mm above a detector with 100  $\mu\text{m}$  pixelation, assuming an input frequency of 2.0 lp/mm and an object velocity of 0  $\mu\text{m/s}$ . As expected, a conventional CTM system with x-ray tube motion at constant angular velocity has much less modulation than a system with step-and-shoot motion (SSM) for any fixed scan time. This finding arises because SSM has no FS blurring. To demonstrate that the newly proposed CTM\* design minimizes the impact of FS blurring, Figure 2(c) shows the increase in modulation of CTM\* relative to conventional CTM. The increase in modulation is most pronounced at values of  $\omega_{\min}$  which approach zero. In fact, at scan times greater than 2.1 s, the relative difference in modulation between SSM and CTM\* is less than 1.0% assuming that  $\omega_{\min} = 0$ .

Although patient motion is not modeled in Figure 2(c), it is studied in Figure 2(d) using an object velocity of 60  $\mu\text{m/s}$  along the mediolateral direction. This object velocity was chosen based on a clinical case investigated in our previous paper.<sup>2</sup> That paper showed that a conventional CTM system with patient motion is optimized by an intermediate scan time. Figure 2(d) illustrates that this trend continues to hold in the newly proposed CTM\* design. The optimal scan time decreases as  $\omega_{\min}$  is reduced. In a SSM system, modulation is optimized by the shortest possible scan time.

### 3.2 Validation Using Computer Breast Phantoms

We validated the benefits of the CTM\* design using x-ray simulations of computer breast phantoms<sup>7</sup> with microcalcifications. In the simulations, the step angle ( $\Delta\psi$ ) was 2.67°, and the voxel size in the computer phantom was 200  $\mu\text{m}$ . The step angle differs slightly from the one used in Figures 1-2; it was chosen due to the current limitations in the simulation platform for the computer phantoms. All other acquisition parameters match those used in Figure 1. To simulate tube motion, we integrated the detector signal over the arc swept by the x-ray tube during each projection. This integration was approximated by a middle sum in which the exposure time for each projection was divided into multiple time points; in our simulation, nine time points were considered. Reconstructions were generated with a commercial prototype backprojection filtering algorithm (Briona<sup>TM</sup>, Real Time Tomography, Villanova, PA).<sup>8</sup>

In a noiseless simulation, Figure 4(a)-(c) shows the slice in the reconstruction corresponding to the depth at which the calcifications are in focus. Pixel size in the reconstruction grid was 10  $\mu\text{m}$ , corresponding to 10-fold magnification. As

expected, calcifications have higher contrast in the SSM image than in the conventional CTM image. For example, at the arrow for which the calcification has an approximate diameter of 300  $\mu\text{m}$ , the relative difference in peak contrast between SSM and conventional CTM is nearly 10%. In a separate study, Shaheen *et al.* calculated a similar difference in peak contrast at a comparable calcification diameter (250  $\mu\text{m}$ ).<sup>1</sup> Their work considered a background consisting exclusively of power-law (*i.e.*, anatomical) noise; this study uses a slightly more realistic breast background that also models glandular and adipose tissue. Importantly, Figure 4 demonstrates that there is minimal difference in contrast comparing SSM and the newly proposed CTM\* design. This finding suggests that the velocity profile of the x-ray tube can be successfully optimized to minimize FS blurring. This simulation was performed assuming  $\omega_{\min} = 0$ . As shown in Figure 1, this choice of  $\omega_{\min}$  yields the smallest tube motion during the acquisition of the projections.

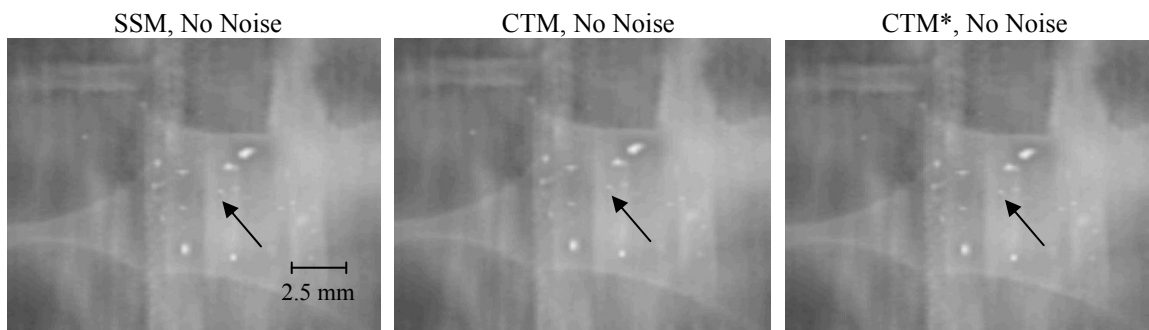


**Figure 4.** Reconstructions were simulated for a computer breast phantom with microcalcifications assuming no noise. As shown by the arrow, the calcification with 300  $\mu\text{m}$  diameter exhibits nearly 10% loss in contrast in the conventional CTM reconstruction relative to the SSM reconstruction. This result is expected since tube motion blurs the image in a conventional CTM system. Conversely, the contrast difference between SSM and the newly proposed design (CTM\*) is minimal.

In Figure 5, the difference in signal comparing all combinations of systems is calculated. Figure 5 shows that tube motion blurs the outlines of structures, since these outlines are seen in the difference image comparing SSM and conventional CTM. A similar result holds in comparing CTM\* and conventional CTM. By contrast, the difference image comparing SSM and CTM\* does not show the outlines of structures, and spans a much smaller range of values. This property is emphasized in box plots of differences between systems (Figure 6); these plots show that SSM and the newly proposed CTM\* design have comparable advantages over a conventional CTM system.

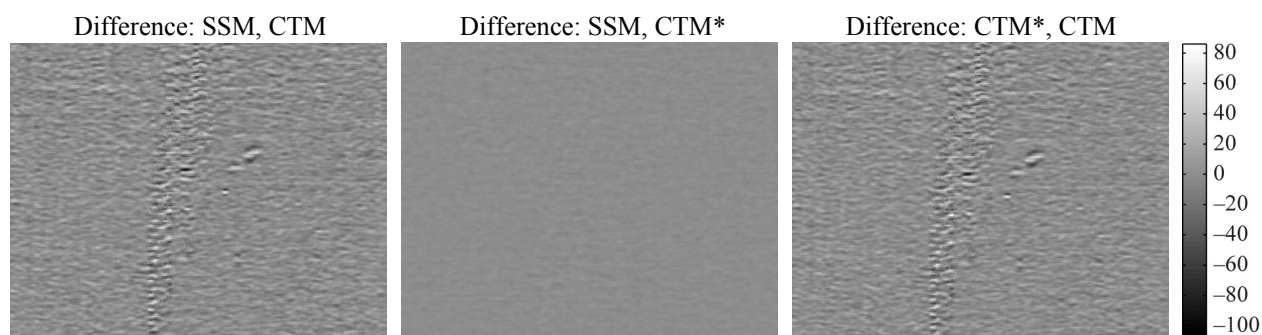


**Figure 5.** Difference images for all combinations of reconstructions in Figure 4 are shown. The difference image comparing SSM and conventional CTM shows the outlines of structures, indicating that tube motion blurs small details in the image.

We next modeled quantum noise in the simulation (Figure 7). With this approach, we found that the contrast difference between SSM and conventional CTM is not consistent among calcifications of a similar size. In plotting the difference image comparing SSM and conventional CTM, it is clear from the color bar that the variation in signal greatly exceeds the variation in the analogous difference image of the noiseless simulation (Figure 5). For this reason, random noise fluctuations can be comparable to the contrast difference between SSM and conventional CTM; a more detailed analysis of the effect of tube motion on signal-to-noise is on-going.

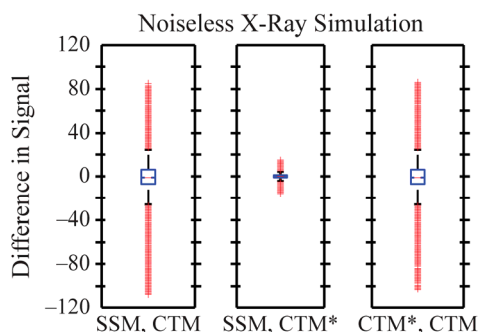


**Figure 6.** Box plots summarizing each difference image in Figure 5 are shown. There is minimal difference between SSM and CTM\*; this result indicates that the newly proposed design reduces the FS blurring found in conventional CTM.

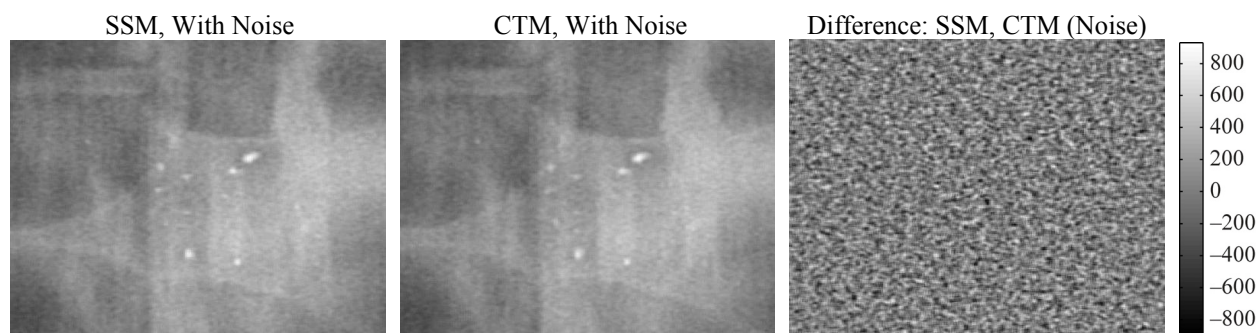


**Figure 7.** Reconstructions are shown with quantum noise, corresponding to  $10^5$  x rays per detector element during the entire DBT scan. The outlines of structures are not evident in the difference image comparing SSM and conventional CTM; this result differs from Figure 5 examining noiseless data.

#### 4. DISCUSSION AND CONCLUSION

There are two main schemes for acquiring projections in DBT, step-and-shoot motion (SSM) and continuous tube motion (CTM). Due to mechanical considerations, SSM systems have much longer scan time than CTM systems. The benefit of a fast acquisition time in a CTM system is minimizing patient motion; the trade-off is FS blurring during the exposure time of each projection.

In clinical CTM systems, the angular velocity of the x-ray tube is constant during the scan time. This work considers the potential benefits of a tube velocity that varies with time. The tube velocity is large between projections and approaches zero during each projection. Using a sinusoidal velocity profile [Figure 1(a)-(b)], it was demonstrated that the newly proposed design minimizes FS blurring, as measured by the tube sweep per projection ( $\Psi$ ). Because this velocity profile is smooth and its high-order derivatives are continuous, a short scan time should continue to be achievable. We believe that the newly proposed design can be implemented in clinical systems using a servo motor.

The reconstruction of a sine plate was analyzed to quantify the improvements in image quality with the newly proposed design. We calculated modulation at a fixed frequency by comparing the amplitude of the reconstruction against the attenuation coefficient of the object. At scan times used in clinical CTM systems (approximately 3.5 s), the relative difference in modulation between SSM and the newly proposed design was found to be less than 1.0%. This result indicates that the newly proposed design can be successfully used to minimize the drawbacks of FS blurring in a CTM system. The benefits of the newly proposed design were validated with reconstructions of microcalcifications in computer breast phantoms. Concordant with previous studies, this work found that conventional CTM reduces the contrast of microcalcifications compared with SSM. This loss of contrast was minimal using the newly proposed design.

In this work, the minimum velocity of the x-ray tube was modeled as a parameter ( $\omega_{\min}$ ) that controls FS blurring during each projection. This paper showed that the maximum tube velocity ( $\omega_{\max}$ ) increases as  $\omega_{\min}$  is reduced [Figure 2(a)]. To achieve the smallest FS blurring ( $\omega_{\min} = 0$ ), the maximum tube velocity must attain twice the value for conventional CTM (i.e.,  $\omega_{\max} = 2\omega_{\text{CTM}}$ ). Because mechanical considerations may place a limit on the maximum tube velocity that is achievable, this result can be interpreted as a mechanical constraint for optimizing the benefits of the newly proposed design.

In noiseless images of the computer breast phantom, it was shown that image acquisition with conventional CTM yields nearly 10% loss of contrast in small microcalcifications compared with SSM. The difference between SSM and conventional CTM can be hidden by the presence of quantum noise (Figure 7). This work has not investigated whether the loss of contrast in the conventional CTM image is sufficiently large to reduce the detectability of the object (a binary decision made by the observer). An observer study will be necessary to determine a threshold for acceptable loss of contrast in a CTM system. Because the loss of contrast is minimal in the newly proposed design at the scan time currently used in clinical DBT systems, future work will investigate whether the scan time can be reduced in the CTM\* design to meet the threshold for acceptable loss of contrast. The benefits of potentially shortening the scan time in the newly proposed geometry are two-fold; reducing the time for compression discomfort, and minimizing the blurring due to patient motion.

A parameter that controls the blurring due to tube motion is the height  $z$  of the object above the detector. In a CTM system, increasing the height  $z$  is expected to broaden the shadow of the object in each projection image. In the analytical model of the sine plate and in the simulated reconstructions of microcalcifications, this work does not investigate the effect of varying the height  $z$ . Future work should investigate whether the loss of contrast in the images of microcalcifications becomes more pronounced with increasing  $z$ . This result will prove to be important for establishing a threshold for acceptable loss of contrast in a CTM system.

In future studies, additional velocity profiles for the x-ray tube should be modeled as techniques for minimizing FS blurring. This work simulates a sinusoidal tube velocity profile [Figure 1(a)-(b)]; to flatten the trough during the exposure time of each projection, higher powers of sine should be considered. In addition, future studies should model the MTF degradation due to the finite size of the focal spot<sup>9</sup> and non-normal x-ray incidence on the detector surface.<sup>10-17</sup> Finally, because the attenuation coefficient of an object is energy-dependent, polyenergetic x rays should also be simulated.

## 5. ACKNOWLEDGEMENT

The authors are grateful to Baorui Ren (Hologic Inc., Bedford, MA) for sharing information on the acquisition geometry of the Selenia Dimensions DBT system. The project described was supported by predoctoral training Grant No. W81XWH-11-1-0100 through the Department of Defense Breast Cancer Research Program. Additional support was provided by the US National Institutes of Health (grant 1R01CA154444). The content is solely the responsibility of the authors and does not necessarily represent the official views of the funding agency.

## 6. REFERENCES

1. Shaheen E, Marshall N, Bosmans H. Investigation of the effect of tube motion in breast tomosynthesis: continuous or step and shoot? Paper presented at: SPIE Medical Imaging, 2011; Lake Buena Vista, FL.
2. Acciavatti RJ, Maidment ADA. Optimization of Continuous Tube Motion and Step-and-Shoot Motion in Digital Breast Tomosynthesis Systems with Patient Motion. Paper presented at: SPIE Medical Imaging, 2012; San Diego, CA.
3. Acciavatti RJ, Maidment ADA. Investigating the Potential for Super-Resolution in Digital Breast Tomosynthesis. Paper presented at: SPIE Medical Imaging, 2011; Lake Buena Vista, FL.
4. Acciavatti RJ, Maidment ADA. Observation of super-resolution in digital breast tomosynthesis. *Medical Physics*. 2012;39(12):7518-7539.
5. Acciavatti RJ, Maidment ADA. Proposing an Acquisition Geometry That Optimizes Super-Resolution in Digital Breast Tomosynthesis. *Lecture Notes in Computer Science*. 2012;7361:386-393.

6. Acciavatti RJ, Mein SB, Maidment ADA. Investigating Oblique Reconstructions with Super-Resolution in Digital Breast Tomosynthesis. *Lecture Notes in Computer Science*. 2012;7361:737-744.
7. Bakic PR, Zhang C, Maidment ADA. Development and characterization of an anthropomorphic breast software phantom based upon region-growing algorithm. *Medical Physics*. 2011;38(6):3165-3176.
8. Kuo J, Ringer PA, Fallows SG, Bakic PR, Maidment ADA, Ng S. Dynamic Reconstruction and Rendering of 3D Tomosynthesis Images. Paper presented at: SPIE Medical Imaging, 2011; Lake Buena Vista, FL.
9. Johns HE, Cunningham JR. Chapter 16: Diagnostic Radiology. *The Physics of Radiology*. 4th ed. Springfield, IL: Charles C Thomas; 1983:557-669.
10. Que W, Rowlands JA. X-ray imaging using amorphous selenium: Inherent spatial resolution. *Medical Physics*. 1995;22(4):365-374.
11. Hajdok G, Cunningham IA. Penalty on the detective quantum efficiency from off-axis incident x rays. Paper presented at: Medical Imaging 2004: Physics of Medical Imaging, 2004; San Diego, CA.
12. Mainprize JG, Bloomquist AK, Kempston MP, Yaffe MJ. Resolution at oblique incidence angles of a flat panel imager for breast tomosynthesis. *Medical Physics*. 2006;33(9):3159-3164.
13. Acciavatti RJ, Maidment ADA. Calculation of OTF, NPS, and DQE for Oblique X-Ray Incidence on Turbid Granular Phosphors. *Lecture Notes in Computer Science*. 2010;6136:436-443.
14. Freed M, Park S, Badano A. A fast, angle-dependent, analytical model of CsI detector response for optimization of 3D x-ray breast imaging systems. *Medical Physics*. 2010;37(6):2593-2605.
15. Freed M, Park S, Badano A. Erratum: "A fast, angle-dependent, analytical model of CsI detector response for optimization of 3D x-ray breast imaging systems" [Med. Phys. 37, 2593-2605 (2010)]. *Medical Physics*. 2011;38(4):2307.
16. Badano A, Freed M, Fang Y. Oblique incidence effects in direct x-ray detectors: A first-order approximation using a physics-based analytical model. *Medical Physics*. 2011;38(4):2095-2098.
17. Acciavatti RJ, Maidment ADA. Optimization of phosphor-based detector design for oblique x-ray incidence in digital breast tomosynthesis. *Medical Physics*. 2011;38(11):6188-6202.